Lasing in ring resonators by stimulated Brillouin scattering in the presence of nonlinear loss

SAYYED REZA MIRNAZIRY,[1,2,*] CHRISTIAN WOLFF,[1,2] M. J. STEEL,[1,3] BLAIR MORRISON,[1,4] BENJAMIN J. EGGLETON,[1,4] AND CHRISTOPHER G. POULTON[1,2]

[1]*Centre for Ultrahigh bandwidth Devices for Optical Systems (CUDOS), Australia*
[2]*School of Mathematical and Physical Sciences, University of Technology Sydney, NSW 2007, Australia*
[3]*MQ Photonics Research Centre, Department of Physics and Astronomy, Macquarie University Sydney, NSW 2109, Australia*
[4]*Institute of Photonics and Optical Science (IPOS), School of Physics, University of Sydney, NSW 2006, Australia*
[*]*Sayyed.R.Mirnaziry@student.uts.edu.au*

Abstract: We theoretically investigate lasing due to stimulated Brillouin scattering in integrated ring resonators. We give analytic expressions and numerical calculations for the lasing threshold for rings in the presence of for both linear and nonlinear loss. We demonstrate the operation of the ring in the different regimes of amplification and lasing, and show how these regimes depend on the coupling to the ring and on the nonlinear parameters. In the case of nonlinear losses, we find that there can exist an upper threshold to the lasing regime where the losses are dominated by free-carrier absorption. We also find that nonlinear losses can inhibit Brillouin lasing entirely for certain ranges of coupling parameters, and we show how the correct ranges of coupling parameters can be calculated and optimized for the design of integrated Brillouin lasers.

References and links

1. R. W. Boyd, *Nonlinear Optics* (Academic Press, 2003).
2. Z. Zhu, D. J. Gauthier, and R. W. Boyd, "Stored light in an optical fiber via stimulated Brillouin scattering," Science **318**, 1748–1750 (2007).
3. M. Nikles, L. Thévenaz, and P. A. Robert, "Simple distributed fiber sensor based on brillouin gain spectrum analysis," Opt. Lett. **21**, 758–760 (1996).
4. J. Geng, S. Staines, Z. Wang, J. Zong, M. Blake, and S. Jiang, "Highly stable low-noise Brillouin fiber laser with ultranarrow spectral linewidth," IEEE Photon. Technol. Lett. **18**, 1813–1815 (2006).
5. R. Pant, D. Marpaung, I. V. Kabakova, B. Morrison, C. G. Poulton, and B. J. Eggleton, "On-chip stimulated Brillouin scattering for microwave signal processing and generation," Laser Photon. Rev. **8**, 653–666 (2014).
6. B. J. Eggleton, C. G. Poulton, and R. Pant, "Inducing and harnessing stimulated Brillouin scattering in photonic integrated circuits," Adv. Opt. Photon. **5**, 536–587 (2013).
7. P. T. Rakich, C. Reinke, R. Camacho, P. Davids, and Z. Wang, "Giant enhancement of stimulated Brillouin scattering in the subwavelength limit," Phys. Rev. X **2**, 011008 (2012).
8. R. Van Laer, B. Kuyken, D. Van Thourhout, and R. Baets, "Interaction between light and highly confined hypersound in a silicon photonic nanowire," Nat. Photon **9**, 199–203 (2015).
9. M. Merklein, A. Casas-Bedoya, D. Marpaung, T. F. Büttner, M. Pagani, B. Morrison, I. V. Kabakova, and B. J. Eggleton, "Stimulated Brillouin scattering in photonic integrated circuits: novel applications and devices," IEEE J. Sel. Top. Quantum Electron. **22**, 336–346 (2016).
10. V. R. Almeida, C. A. Barrios, R. R. Panepucci, and M. Lipson, "All-optical control of light on silicon chip," Nature **431**, 1081 (2004).
11. S. Azzini, D. Grassani, M. Galli, L. C. Andreani, M. Sorel, M. J. Strain, L. Helt, J. Sipe, M. Liscidini, and D. Bajoni, "From classical four-wave mixing to parametric fluorescence in silicon microring resonators," Opt. Lett. **37**, 3807–3809 (2012).

12. M. Ferrera, L. Razzari, D. Duchesne, R. Morandotti, Z. Yang, M. Liscidini, J. Sipe, S. Chu, B. Little, and D. Moss, "Low-power continuous-wave nonlinear optics in doped silica glass integrated waveguide structures," Nat. Photon. **2**, 737–740 (2008).

13. B. Morrison, A. Casas-Bedoya, G. Ren, K. Vu, Y. Liu, A. Zarifi, T. G. Nguyen, D.-Y. Choi, D. Marpaung, S. J. Madden, A. Mitchell, and B. J. Eggleton, "Compact Brillouin devices through hybrid integration on silicon," Optica **4**, 847–854 (2017).

14. G. Lin, S. Diallo, K. Saleh, R. Martinenghi, J.-C. Beugnot, T. Sylvestre, and Y. K. Chembo, "Cascaded Brillouin lasing in monolithic barium fluoride whispering gallery mode resonators," Appl. Phys. Lett. **105**, 231103 (2014).

15. J. Li, H. Lee, and K. J. Vahala, "Low-noise Brillouin laser on a chip at 1064 nm," Opt. Lett. **39**, 287–290 (2014).

16. I. V. Kabakova, R. Pant, D.-Y. Choi, S. Debbarma, B. Luther-Davies, S. J. Madden, and B. J. Eggleton, "Narrow linewidth Brillouin laser based on chalcogenide photonic chip," Opt. Lett. **38**, 3208–3211 (2013).

17. L. Stokes, M. Chodorow, and H. Shaw, "All-fiber stimulated Brillouin ring laser with submilliwatt pump threshold," Opt. Lett. **7**, 509–511 (1982).

18. J. C. Yong, L. Thévenaz, and B. Y. Kim, "Brillouin fiber laser pumped by a DFB laser diode," J. Lightwave Technol. **21**, 546 (2003).

19. S. R. Mirnaziry, C. Wolff, M. Steel, B. J. Eggleton, and C. G. Poulton, "Stimulated Brillouin scattering in integrated ring resonators," J. Opt. Soc. Am. B **34**, 937–949 (2017).

20. F. De Leonardis, B. Troia, R. A. Soref, and V. M. Passaro, "Theoretical demonstration of Brillouin lasing effect in racetrack resonators based on germanium waveguides in the mid-infrared," Opt. Lett. **41**, 416–419 (2016).

21. W. Loh, A. A. Green, F. N. Baynes, D. C. Cole, F. J. Quinlan, H. Lee, K. J. Vahala, S. B. Papp, and S. A. Diddams, "Dual-microcavity narrow-linewidth Brillouin laser," Optica **2**, 225–232 (2015).

22. S. Spillane, T. Kippenberg, and K. Vahala, "Ultralow-threshold raman laser using a spherical dielectric microcavity," Nature **415**, 621–623 (2002).

23. T. J. Kippenberg, S. M. Spillane, B. Min, and K. J. Vahala, "Theoretical and experimental study of stimulated and cascaded raman scattering in ultrahigh-q optical microcavities," IEEE J. Sel. Top. Quantum Electron. **10**, 1219–1228 (2004).

24. C. Wolff, P. Gutsche, M. J. Steel, B. J. Eggleton, and C. G. Poulton, "Impact of nonlinear loss on stimulated Brillouin scattering," J. Opt. Soc. Am. B **32**, 1968–1978 (2015).

25. A. Yariv, "Universal relations for coupling of optical power between microresonators and dielectric waveguides," Electron. Lett. **36**, 321–322 (2000).

26. S. R. Mirnaziry, C. Wolff, M. Steel, B. J. Eggleton, and C. G. Poulton, "Stimulated Brillouin scattering in silicon/chalcogenide slot waveguides," Opt. Express **24**, 4786–4800 (2016).

27. D. G. Rabus, *Integrated Ring Resonators* (Springer, 2007).

28. W. R. McKinnon, D.-X. Xu, C. Storey, E. Post, A. Densmore, A. Delâge, P. Waldron, J. H. Schmid, and S. Janz, "Extracting coupling and loss coefficients from a ring resonator," Opt. Express **17**, 18971–18982 (2009).

29. R. G. Smith, "Optical power handling capacity of low loss optical fibers as determined by stimulated Raman and Brillouin scattering," Appl. Opt. **11**, 2489–2494 (1972).

1. Introduction

Stimulated Brillouin Scattering (SBS) is a strong nonlinear interaction between optical fields whereby energy is transferred between closely-spaced spectral lines by means of hypersonic waves [1]. SBS is important in several photonics applications, including the fast processing of radio-frequency signals [2], sensing [3], and the generation of ultra-narrow-linewidth sources [4, 5]. Of particular interest is the use of SBS in integrated platforms, which give significant advantages in terms of stability and device size [6]. Although the SBS gain can be significantly enhanced in nanowire waveguides [7], achieving useful levels of Stokes amplification still requires relatively high pump powers and waveguide lengths on the order of centimeters [8, 9]. One way of circumventing these limitations is to use high quality-factor integrated ring resonators, where the build-up of power in on-resonance pump and Stokes waves can dramatically improve input power requirements. Ring resonators are commonly employed to enhance nonlinear effects in a range of photonics applications [10–12], and recent experiments have demonstrated SBS in hybrid silicon-chalcogenide racetrack structures [13] and Whispering Gallery Mode (WGM) resonators [14]. The combination of a high-Q cavity and gain also opens up the possibility of SBS lasing, which is essential for many of the proposed SBS-based applications [15, 16]; SBS lasing has thus far been demonstrated in fibre ring structures [17, 18], and integrated ring resonators have recently been proposed both for SBS-based amplification [19] and for lasing [20, 21].

Despite these recent studies, a quantitative picture of the physics of SBS lasing in integrated ring resonators, including such important effects as nonlinear losses, does not yet exist in the literature. Although several papers give expressions for the lasing threshold for the closely-related case of Raman scattering (see for example [22, 23]) and these expressions have been used (though without a formal derivation) in SBS lasing experiments [13], it is not known in which situations these formulas can be correctly applied, and a full derivation of the lasing threshold for SBS in integrated ring structures is currently lacking. As a result is sometimes not clear as to exactly when lasing occurs for SBS, as distinct from regimes where the Stokes signal is strongly amplified. This distinction is particularly problematic in semiconductor platforms, in which nonlinear losses, in particular Free-Carrier Absorption (FCA), can significantly affect the physics of the SBS interaction and will strongly affect the achievable SBS gain [24]. In the case of straight waveguides, nonlinear losses lead to the existence of an optimal waveguide length for SBS gain, as well as a maximum amplification of the Stokes signal; it is not immediately clear how these effects carry over to ring resonators, and how these losses affect the transition from SBS amplification to SBS lasing.

Here we theoretically and numerically investigate SBS lasing in ring resonators in the presence of linear and nonlinear optical loss. This analysis provides a better understanding of the lasing mechanism in rings with materials such as silicon or germanium in which higher order optical losses are non-negligible. We adopt the formalism outlined in [19], in which techniques were given for the computation of SBS in the amplification regime. Building on that work, we here study the different regimes of operation of the ring while focussing on the transition between amplification and lasing, and compute the threshold powers for this transition in the presence of nonlinear losses. We derive analytic expressions for the lasing threshold and investigate the effect of nonlinear losses. This derivation follows that of [25], in which the threshold is derived without noise initiation of the Stokes. While the derivation of the lasing threshold follows from a small-signal approximation, we also provide and analyse a full model including the large signal terms, and compute the Stokes amplification and the Stokes output power for realistic ring resonator parameters. These results can therefore be used for resonator design and for comparison with experimental results. We also discuss the physics of SBS lasing in rings: in rings with nonlinear loss we show that there exists a finite power interval over which lasing occurs; we compute this interval and provide design parameters that can be used for SBS-based ring resonator structures. Our study is in particular useful for realizing SBS lasing in chip scale devices. It provides sufficient information about optimum cavity inputs/outputs as well as the required physical parameters, optical and acoustic properties in a ring configuration to be used in designing integrated racetrack resonators for SBS lasing.

2. Geometry and numerical computations

Following [19], we consider the geometry of a ring resonator sketched in Fig. 1. A ring of length L is coupled to a single straight waveguide via a coupling region; for the sake of simplicity we assume that the SBS gain occurs only in the ring section and not in the coupler. Here we consider the backward SBS process, in which input pump P_p^{in} and Stokes P_s^{in} contra-propagate; the forward SBS process can be handled using the same formalism, appropriately modified to account for the different propagation direction. This modification however, does not lead to a change in the magnitude of resultant threshold powers or in output Stokes demonstrated in this paper, assuming identical gain, loss coefficients, coupling and physical properties (i.e. ring length) in the Forward SBS process to those of backward SBS.

Throughout this investigation we are assuming that the pump and the Stokes are aligned to two cavity modes, and that the free-spectral-range (FSR) of the ring is equal to an integer multiple of the Brillouin shift. Resonant coupling Brillouin lasers are in particular efficient — in terms of the required pump power to achieve lasing — for chip scale ring resonators in

which pump and Stokes frequencies are designed to lie on close resonances of the cavity. In practice nonlinear dispersion (Kerr, free-carrier dispersion, and frequency pulling due the phase shift arising from the SBS process itself) as well as thermal effects can result in a change in the FSR of the cavity, however for typical power levels (as discussed in [26]) such changes are far smaller than the SBS linewidth and can be neglected. The absolute values of the cavity mode frequencies are however expected to shift markedly. We therefore assume that active stabilisation of the pump is used to track the frequency of the cavity mode; the shift of the Stokes frequency will then automatically continue to lie on-resonance. Note that this implicitly assumes that the variation in pump power is slow enough to accommodate thermal effects; throughout this paper we therefore operate in the quasi-CW regime, in which it is assumed that the pulse lengths are much longer than the phonon lifetime — in most platforms this is on the order of 10 ns. A study of full dynamic response, including the stability, of these devices we leave to future investigations.

The powers in the pump and Stokes within the ring are then governed by the equations [24]

$$\frac{dP_p}{dz} = -(\alpha + \beta P_p + \gamma P_p^2)P_p - (2\beta + 4\gamma P_p + \gamma P_s + \Gamma)P_p P_s, \tag{1}$$

$$\frac{dP_s}{dz} = (\alpha + \beta P_s + \gamma P_s^2)P_s + (2\beta + 4\gamma P_s + \gamma P_p - \Gamma)P_p P_s, \tag{2}$$

where P_p and P_s are the circulating pump and Stokes powers, respectively; α, β and γ are the linear, TPA and FCA-induced loss coefficients respectively, and Γ is the SBS gain expressed in units of $W^{-1}m^{-1}$. We also note that pump and Stokes powers take positive values in our model, as opposed to the formalism where counter-propagating waves have negative powers [24]. We have assumed here also that both pump and Stokes are in the same optical mode, and so the nonlinear coefficients are identical in both equations; this is realistic given the close spectral spacing of pump and Stokes for the SBS interaction, but could be generalized at the expense of complicating the formulation. Furthermore, in Eqs. (1) and (2) we have not considered noise, as arising from spontaneous emission or from thermal phonons. As a result, this model does not allow noise-related predictions, such as the linewidth in the lasing regime. The focus of this work is to study the dependence of the lasing threshold on the various system parameters including coupling, nonlinear loss and pump power. A corresponding study of the noise properties, beginning from the coupled amplitude equations, is beyond the scope of this current work.

On resonance, the values of the pump power at the beginning ($z = 0$) and at the end ($z = L$) of the ring segment are related to the input pump power by [19]

$$P_p^{in} = \frac{1}{|\kappa|^2}\left(\sqrt{P_p(0)} - |\tau|\sqrt{P_p(L)}\right)^2, \tag{3}$$

where κ and τ are the complex envelope coupling coefficients as depicted in Fig. 1, related by $|\tau|^2 + |\kappa|^2 = 1$ [25, 27]. Similarly, the values of the Stokes are related via the coupling region by

$$P_s^{in} = \frac{1}{|\kappa|^2}\left(\sqrt{P_s(L)} - |\tau|\sqrt{P_s(0)}\right)^2. \tag{4}$$

In writing Eqs. (3) and (4) we have implicitly assumed the coupling coefficients κ and τ are the same for both pump and Stokes and do not change with frequency over very small (GHz) ranges studied here. The system of Eqs. (1)-(4) encapsulates the physics of the ring operation: the input pump is transferred to the ring at $z = 0$, experiences both linear and nonlinear loss as well as loss to the other mode, and then is partially transferred to the output. The Stokes on
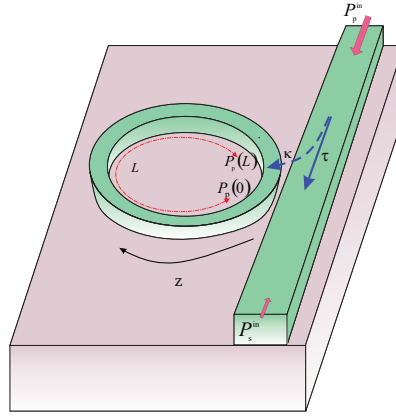
Fig. 1. Schematic of a ring resonator in vicinity of a straight coupler.
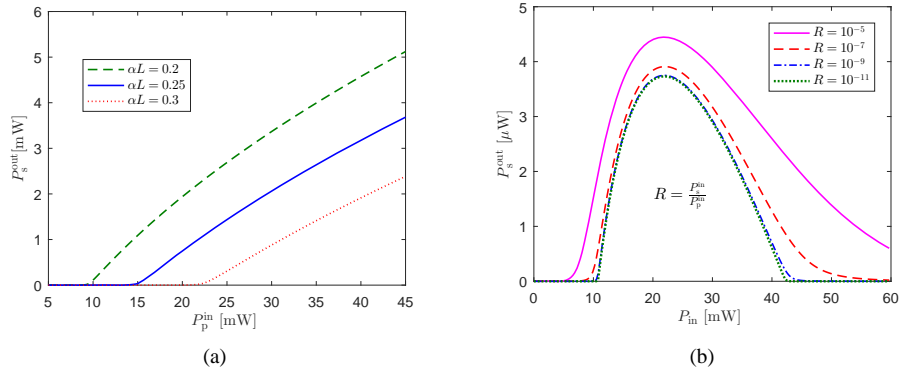

(a)

(b)

Fig. 2. Output Stokes power as a function of input pump power at the lasing region and resonant condition in the presence of (a) linear losses and (b) both linear and nonlinear losses. In (a) $\Gamma = 500$ $W^{-1}m^{-1}$, $R = 10^{-11}$ and $\kappa = 0.31$. In (b) $\alpha L = 0.2$; $\gamma = 1.8 \times 10^5$ $W^{-2}m^{-1}$, $\beta = 10$ $W^{-1}m^{-1}$, $\kappa = 0.16$ and $\Gamma = 4000$ $W^{-1}m^{-1}$. The length $L = 10.879$ mm corresponds a ring resonator with free spectral range equal to a Brillouin frequency shift of 10 GHz.

the other hand is input at $z = L$ and experiences gain with decreasing z, as well as linear and nonlinear loss.

Figure 2 shows the output Stokes power resulting from the numerical solution of Eq. (1)-(4), for a ring resonator with (a) linear losses only, and (b) with both linear and nonlinear losses. To solve these equations we apply the numerical approach presented in [19] in which pump and Stokes are computed using an iterative shooting technique, by which the differential equations are solved at each step of the iteration using a Runge-Kutta method, and the mismatch in the boundary conditions becomes a measure of the closeness to the true solution. In Fig. 2(a) the output Stokes is computed for a ring with $\Gamma = 500 \text{ W}^{-1}\text{m}^{-1}$ keeping the coupling constant fixed at $\kappa = 0.31$ and changing the values of αL in order to highlight the impact of the linear loss. A clear threshold pump power can be seen, denoted by a sharp increase in Stokes power; the value of this threshold increases with the linear loss. The effect of nonlinear losses can be seen in the example shown in Fig. 2(b). Here we have assumed that $\alpha L = 0.2$; $\gamma = 1.8 \times 10^5 \text{ W}^{-2}\text{m}^{-1}$, $L = 10.879$ mm, $\Gamma = 4000 \text{ W}^{-1}\text{m}^{-1}$, which are close to experimentally-realisable values for a silicon nanophotonic waveguide, and we have neglected TPA ($\beta = 0 \text{ W}^{-1}\text{m}^{-1}$), which has a negligible direct effect on SBS in silicon. The Stokes power is depicted as a function of input pump power for different values of the ratio between input pump and Stokes, denoted by $R = P_\text{s}^\text{in}/P_\text{p}^\text{in}$. In order to have an idea for the order of magnitude of R in the lasing regime, we can assume that only a single Stokes photon is initializing the lasing. Then

$$R = \frac{P_\text{s}^\text{in}}{P_\text{p}^\text{in}} = v_\text{g} \frac{h f_\text{s}}{P_\text{p}^\text{in}}, \tag{5}$$

where v_g is the optical group velocity and $h f_\text{s}$ is the Stokes photon energy (h Plank's constant and f_s Stokes frequency). As in the linear case (Fig. 2(b)), the Stokes increases rapidly with the input pump beyond threshold. This trend however is reversed after the Stokes power rises to a maximum value; thereafter, the Stokes power decreases as nonlinear losses begin to dominate. For smaller power ratios R, the Stokes falls abruptly to negligible values once a second, higher threshold is crossed. For higher power ratios, we see that there is no distinct threshold, instead we find that with increasing pump power the amplification of the Stokes signal decreases steadily.

Both thresholds are associated with transitions between lasing and amplification regimes. In the amplification regime the output Stokes is proportional to the input Stokes signal, with gain arising from SBS-induced transfer of energy from the pump. In the lasing regime an infinitely small Stokes signal can generate a finite Stokes output — in a real device, this input Stokes would arise from quantum fluctuations. In this situation the Stokes signal is necessarily far smaller than the pump, and so it is useful to consider the Small Signal Approximation (SSA); under this approximation Eqs. (1) and (2) take the simpler form of [24]

$$\frac{dP_\text{p}(z)}{dz} = -\left(\alpha + \beta P_\text{p}(z) + \gamma P_\text{p}^2(z)\right) P_\text{p}(z), \tag{6}$$

$$\frac{dP_\text{s}(z)}{dz} = \left(\alpha + \gamma P_\text{p}^2(z) - (\Gamma - 2\beta) P_\text{p}(z)\right) P_\text{s}(z). \tag{7}$$

The lasing threshold corresponds to input pump powers for which the Stokes output, when computed using the SSA, tends to infinity. This divergence means that the final value of the Stokes signal, as arising from the full equations (1) and (2), cannot in principle depend on the strength of an initial small signal.

3. Thresholds for rings with linear losses only

We can gain insight into the values at which the thresholds occur by considering the loss and gain mechanisms that act on the Stokes signal within the ring. There are different regimes of behaviour, depending on the value of the round-trip envelope gain G of the Stokes, defined as

$$G = \sqrt{\frac{P_s(0)}{P_s(L)}} . \tag{8}$$

The different modes of operation are reflected in the overall change of the Stokes signal as it passes through the entire device. The net Stokes amplification through the bus, defined as the ratio of output Stokes power from the bus to the input Stokes power, can be expressed as a function of G by [19]:

$$\mathcal{A} := \frac{P_s^{\text{out}}}{P_s^{\text{in}}} = \left| \frac{|\tau| - G}{1 - |\tau|G} \right|^2, \tag{9}$$

For a ring with linear losses we find three different regimes of operation, depending on the value of G in the SSA. Figure 3(a) shows these regimes schematically as a function of input pump power. For $G < 1$, the output Stokes is attenuated ($\mathcal{A} < 1$) because the power conversion from SBS is still too weak to achieve any Stokes enhancement. For values $1 < G < 1/|\tau|$, the SBS gain mechanism is strong enough to compensate the optical losses in the cavity, but is not strong enough for lasing to occur. This is the amplification region, in which the output Stokes from the ring will be proportional to the input Stokes, with amplification factor $\mathcal{A} > 1$ taking a finite value greater than 1. The amplification region has been explored in detail in [19]. As G approaches $1/|\tau|$ the net Stokes amplification tends towards infinity, so that a finite Stokes value is attained even for a vanishingly small input Stokes signal. The input pump power for which this occurs is the lasing threshold. If we include the impact of pump depletion (thereby abandoning the SSA) by solving Eqs. (1) and (2), we find that G remains below $1/|\tau|$ for all pump powers, and therefore from Eq. (9) the Stokes amplification saturates (as shown by the solid line in Fig. 3(a)). However to compute the lasing threshold the SSA is sufficient: a general expression for G in the case of the SSA can be obtained by writing Eq. (7) as $\frac{dP_s}{dz} = -g(z)P_s$, where $g(z) = \left(\alpha + \gamma P_p^2(z) - (\Gamma - 2\beta)P_p(z) \right)$, so that

$$G = \exp \left[\frac{1}{2} \int_0^L g(z)dz \right]. \tag{10}$$

Combining Eq. (9) and Eq. (10), the most general condition for the lasing threshold is then

$$|\tau| \exp \left[\frac{1}{2} \int_0^L g(z)dz \right] = 1. \tag{11}$$

Figure 3(b) compares the Stokes amplification $\mathcal{A}$ predicted by the full model to the amplification computed with the SSA using the parameters illustrated in Fig. 2(a). From the figure it can be seen that the lasing threshold is a monotonic function of the linear loss and shifts to larger pump powers as αL increases and more power is required to compensate the loss. The maximum amplification however does not significantly vary with loss and is mainly a function of coupling coefficients and the power ratio R [19].

An analytic expression for the small signal G can be derived in the linear case; by solving Eq. (6) for $\beta = 0$ and $\gamma = 0$, then substituting into Eq. (7) [19], we find that:

$$G = \exp \left[-\frac{\alpha L}{2} + \frac{\Gamma}{2\alpha} P_p(0)(1 - e^{-\alpha L}) \right]. \tag{12}$$
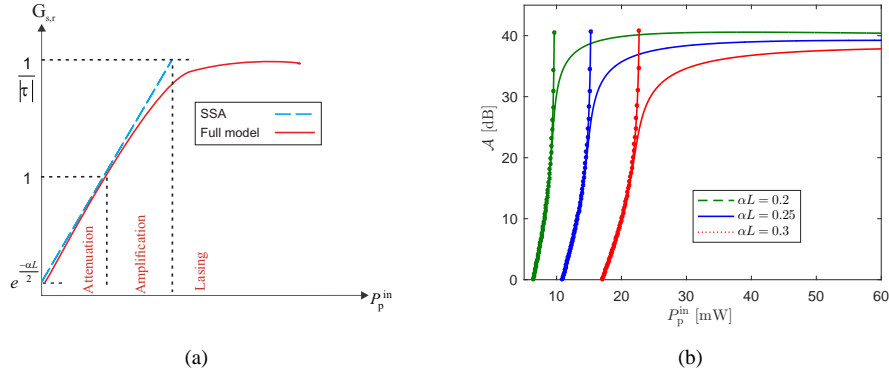
(a)

(b)

Fig. 3. (a) Schematic variation of the round-trip gain in a ring resonator with linear loss within the SSA and full model. (b) The corresponding Stokes total amplification of a ring resonator with the parameters described in Fig. 2(a). The solid circle lines show $\mathcal{A}$ for the small signal model.

Now by substituting G into Eq. (11) and using Eq. (3), the lasing threshold is given by

$$P_p^{\text{in,th}} = \frac{\left(\alpha L - 2\ln|\tau|\right)}{(1 - e^{-\alpha L})} \frac{\alpha}{\Gamma} \frac{(1 - |\tau|e^{(-\alpha L/2)})^2}{|\kappa|^2}, \tag{13}$$

Figure 4(a) shows the contours of normalized pump power $P_p^{\text{in,th}} \frac{\Gamma}{\alpha}$ as a function of αL and $|\kappa|$. We have assume that αL varies between 0 and 1; the reason for this is that for $L = 1\,\text{cm}$ — which is corresponding to a Brillouin frequency of about $10\,\text{GHz}$ in conventional waveguides — then α varies between $0\,\text{dBCm}^{-1}$ to $\sim 4.35\,\text{dBCm}^{-1}$ as a typical range for the linear loss coefficient. While Fig. 4(a) takes into account the SBS lasing, we note that very similar contours are also obtained for the required Stokes power to initialize Stokes amplification [19]. From the figure the threshold power increases with αL as additional power is needed to overcome the losses in the ring. Similarly, the threshold power decreases with the SBS gain (because a higher gain will compensate losses at lower power levels), however achieving lasing is feasible at any value of Γ. We also note that, for a given value of αL, the threshold experiences a minimum as a function of the coupling coefficient $|\kappa|$ at the critical coupling point. Below and above this point the ring is under/over-coupled and the total pump power in the ring will be reduced in comparison to the critical point.

In practice, one has to measure the optical loss and coupling parameters of a ring to be able to determine threshold by Eq. (13). While there are methods to evaluate these quantities [28], Eq. (13) can also be expressed in terms of the optical quality factor [22,23]. The loaded Q factor of the ring can be calculated via (see the Appendix)

$$Q_L = \frac{\sqrt{2}\pi L n_{\text{eff}}}{2\lambda} \frac{\sqrt{1 + |\tau|^2 e^{-\alpha L}}}{1 - |\tau|e^{-\frac{\alpha L}{2}}}, \tag{14}$$

where n_{eff} is the effective index of the ring. Now assuming $\alpha L \ll 1$ and small $|\kappa|$, Eq. (13) simplifies to

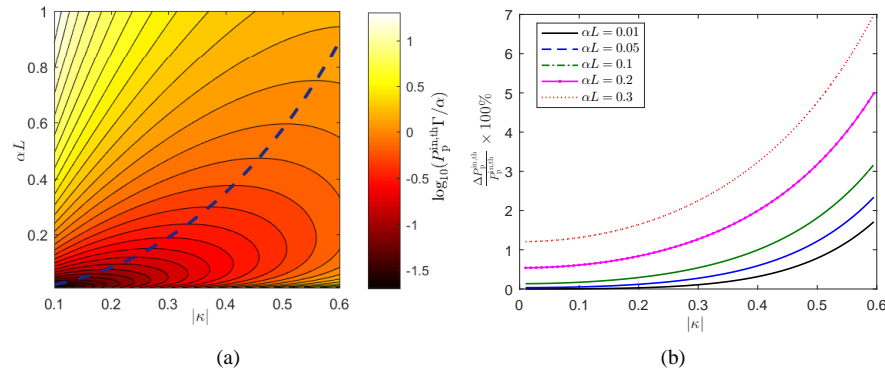$$P_p^{\text{in,th}} = \frac{\pi^2 n_{\text{eff}}^2}{\lambda^2} \frac{L}{\Gamma} Q_c \frac{1}{Q_L^3}, \tag{15}$$

Fig. 4. (a) Contours of the lasing threshold as a function of αL and the coupling coefficient. The dashed line shows the critical coupling. (b) The threshold difference $\Delta P_{\mathrm{p}}^{\mathrm{in,th}}$ between the power obtained by Eq. (13) with the threshold estimated from 15, plotted for a range of the coupling coefficient $|\kappa|$ and for different values of αL. $\Delta P_{\mathrm{p}}^{\mathrm{in,th}}$ is normalized to the exact theoretical value of the threshold (i.e. Eq. (13)) and is plotted in percentage.

where Q_{c} is the Q factor due to the coupling which is given by

$$Q_{\mathrm{c}} = \frac{\sqrt{2}\pi L n_{\mathrm{eff}}}{2\lambda} \frac{\sqrt{1+\tau^2}}{1-\tau}. \tag{16}$$

Equation (15) has also been derived in [22] for Raman sources: it shows the inverse square dependency of the threshold power to the loaded Q-factor in the case where $Q_{\mathrm{L}} = Q_{\mathrm{c}}$. Figure 4(b) shows the difference between the threshold results obtained by Eq. (13) and Eq. (15) for different values of αL. Here, $\Delta P_{\mathrm{p}}^{\mathrm{in,th}} = P_{\mathrm{p}}^{\mathrm{in,th}}[\mathrm{Eq.}\ (13)] - P_{\mathrm{p}}^{\mathrm{in,th}}[\mathrm{Eq.}\ (15)]$ which is normalized to $P_{\mathrm{p}}^{\mathrm{in,th}}[\mathrm{Eq.}\ (13)]$. From the figure, there is a very good agreement between the threshold values for small values of αL and $|\kappa|$ because Eq. (15) is obtained based on these assumptions. $\Delta P_{\mathrm{p}}^{\mathrm{in,th}}$ then grows for larger loss and coupling coefficients.

4. Thresholds for rings with both linear and nonlinear losses

We have seen in Section 2 that the round-trip gain G is greatly affected by the degree of optical loss in the ring. Depending on the strength of nonlinear loss relative to the linear loss, three different scenarios can be attained for the round trip gain. These situations are shown schematically in Fig. 5(a). The first possibility is that the nonlinear loss is negligible at weak pump powers, leading to a similar threshold to that of the linear case, but dominates as the pump power increases. Within the SSA there are two lasing thresholds (pink dashed lines): the SBS gain mainly compensates the linear loss to reach the lower lasing threshold, while for higher powers the nonlinear loss term γP_{p}^2 grows quadratically with the pump power until it is comparable with α in Eq. (7), upon which the second threshold is reached. This leads to a finite lasing interval for the ring; while within the SSA the Stokes power tends to infinity on the edges of this interval (and is not physically meaningful within the interval itself), in the full model G is prevented by the loss terms from reaching the line $1/|\tau|$ and hence the output Stokes power remains finite. This behaviour is shown by numerical calculations of a case study in Fig. 5(b), in which the lasing interval is clearly seen as the flat region for the output Stokes signal. The Stokes is shown for different values of R; while this formally represents an input Stokes seed, this can be shown to be equivalent to a distributed initiation via spontaneous emission [29].
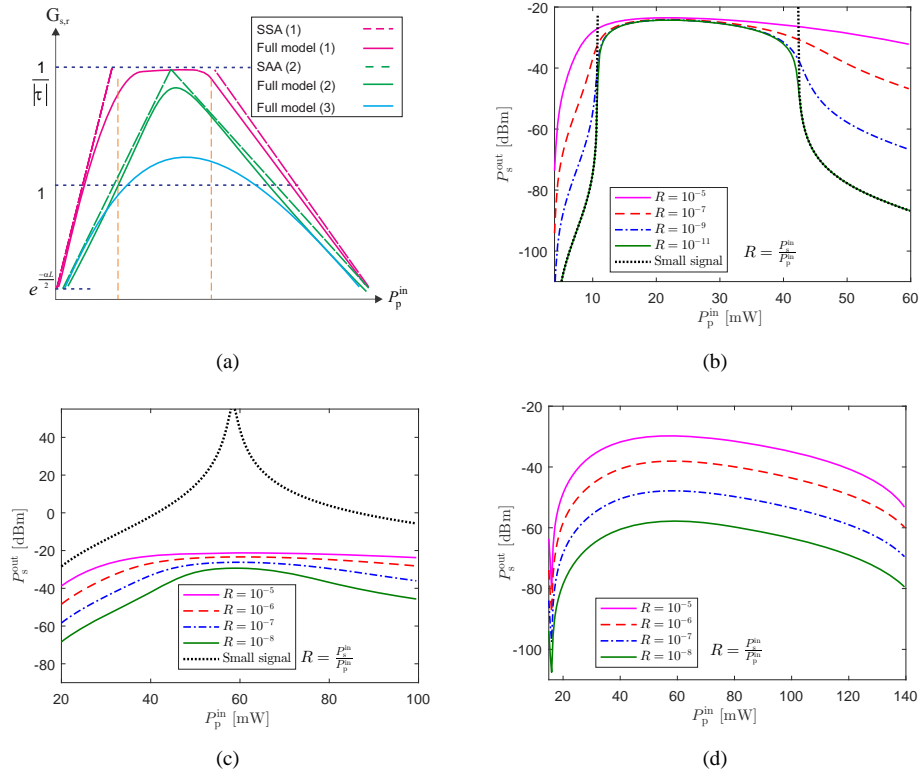
Fig. 5. (a) Schematic variation of the round-trip gain in a ring resonator with nonlinear loss in three different operating regimes shown in pink (with two lasing thresholds), green (with single threshold) and blue (no lasing). Dashed lines show the result of the small signal model and the solid lines are expected in the full model. (b) An example of the Stokes output power for a ring with two lasing thresholds. The black dotted lines shows the SSA. The results of the full model are also shown for different values of the power ratio R. for a ring with the SBS gain and loss parameters described in Fig. 2(b). (c) The Stokes output power for a ring with parameters which leads to a single lasing threshold. $\Gamma = 5970 \text{ W}^{-1}\text{m}^{-1}$; $|\kappa| = 0.24$; $\alpha = 40.9 \text{ m}^{-1}$ and $\gamma = 1.8 \times 10^5 \text{ W}^{-2}\text{m}^{-1}$. (d) The Stokes output power in a ring with parameters that leads to only Stokes amplification. $\Gamma = 5700 \text{ W}^{-1}\text{m}^{-1}$ and the loss and coupling parameters are as in (c).

In the second scenario, the effect of nonlinear loss grows such that it is comparable with the linear loss at the first threshold, and both effects combine to compensate the gain for a single power (green lines in Fig. 5(a)). In this situation lasing will only formally occur for a single input power; beyond this point nonlinear effects will dominate the behaviour. In this situation certain signatures of lasing, such as a linear increase beyond threshold, will not appear — as shown in Fig. 5(c) the Stokes power remains flat at the threshold and decreases thereafter.

In the third scenario (Fig. 5(a), blue line) the value of the round trip gain is clamped by the nonlinear terms to values below the line $1/|\tau|$. In this case the nonlinear losses dominate to the extent that lasing is entirely forbidden. Amplification of the Stokes signal is still however possible if G takes values larger than unity. This is shown in Fig. 5(d), in which the output Stokes grows in proportion to the input Stokes.

Analytic expressions

We now derive expressions for the round trip gain G, and threshold powers, for the case of rings having both linear and nonlinear losses. As in the linear case, the starting point for threshold calculations is the SSA. In the following we neglect the TPA coefficient β as this loss term is small compared to FCA loss in technologically important semiconductors such as silicon. Following the notation in [19] we define a dimensionless parameter $V = P_p(0)\sqrt{\frac{\gamma}{\alpha}}$ which is a normalised measure of the power in the ring. The governing equation for the pump (6) can be solved analytically; the solution is

$$P_p(z) = \sqrt{\frac{\alpha}{\gamma}} \frac{V}{\sqrt{(1+V^2)e^{2\alpha z} - V^2}}. \tag{17}$$

Now by substituting into Eq. (7), G is given by

$$G = \left(\frac{1}{V^2 + 1 - V^2 e^{-2\alpha L}}\right)^{\frac{1}{4}} \exp\left[-\frac{\alpha L}{2} - \mathcal{F} \arctan\left(\frac{V - V\sqrt{(V^2+1)e^{2\alpha L} - V^2}}{V^2 + \sqrt{(V^2+1)e^{2\alpha L} - V^2}}\right)\right], \tag{18}$$

where $\mathcal{F} = \frac{\Gamma}{2\sqrt{\alpha\gamma}}$ is the SBS nonlinear figure of merit [24].

Unlike Eq. (12), G is now a complicated function of three parameters V, αL and $\mathcal{F}$. To evaluate the lasing threshold, we substitute Eq. (18) into Eq. (10) and then use Newton's method to determine the solutions of Eq. (11). Figure 6 shows the contours of $V^{\min}$ and $V^{\max}$, corresponding to the first and second lasing threshold respectively, as functions of the universal ring parameters αL and κ, for typical SBS Figures of Merit $\mathcal{F} = 1.1$ ((a),(b)) and $\mathcal{F} = 1.5$ ((c),(d)). It can be seen in Figs. 6(a) and 6(b) that for a constant αL, $V^{\min}$ increases while $V^{\max}$ decreases with the coupling coefficient $|\kappa|$. This can be understood from the interpretation of $V^{\min,\max}$ as measuring the minimum/maximum powers permissible for lasing in the ring: as the coupling increases toward the critical coupling point, the overall power in the ring increases, making it easier to achieve lasing if only linear losses are dominant, but harder if nonlinear losses are significant. As we approach the amplification region $V^{\min}$ and $V^{\max}$ become closer: the lasing power interval becomes smaller until there only exists a single threshold. The interval is widest in the weakly-coupled regime; this is therefore the most promising configuration for SBS lasing in the presence of nonlinear loss. In addition, comparing the contours of Vth at $\mathcal{F} = 1.1$ with the ones in $\mathcal{F} = 1.5$ reveals that SBS lasing can be achieved across wider ranges of αL and $|\kappa|$ for larger values of $\mathcal{F}$. In addition, the lasing power interval in weakly-couled regimes is further expanded.

The quantity V^{th}, defined as either $V^{\min}$ or $V^{\max}$ as required, can be used to determine the threshold pump power required for lasing. By substituting Eq. (17) into Eq. (3), the lasing threshold(s) can be expressed in terms of input pump power
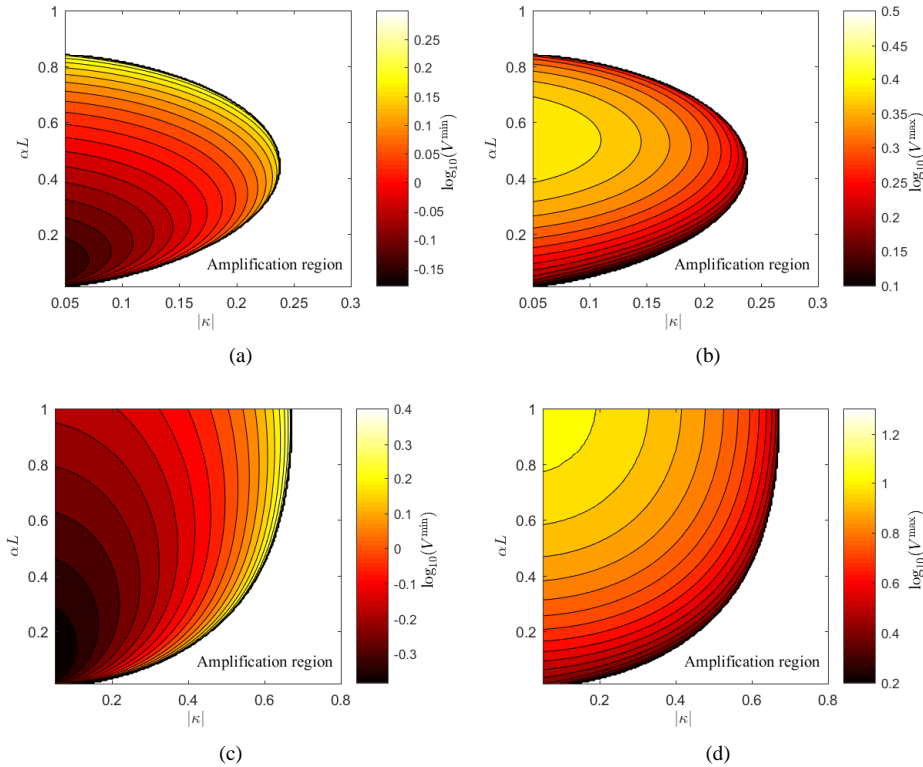
Fig. 6. $V^{\min}$ and $V^{\max}$ at the lasing threshold as a function of κ and αL for (a,b) $\mathcal{F} = 1.1$ and (c,d) $\mathcal{F} = 1.5$.

$$P_p^{\text{in,th}} = \sqrt{\frac{\alpha}{\gamma}} \frac{V^{\text{th}}}{\sqrt{|\kappa|}} \left(1 - |\tau| \sqrt[4]{\frac{1}{((V^{\text{th}})^2 + 1)e^{2\alpha L} - (V^{\text{th}})^2}}\right), \tag{19}$$

Assuming that the physical parameters of the ring remain fixed and hence the ratio α/γ remains constant, we see that $P_p^{\text{in,th}}$ is approximately proportional to V^{th}. For a given figure of merit, a low ratio of α/γ leads to a smaller threshold power as well as a smaller threshold interval, as measured in terms of the parameters of the ring. In Fig. 7 the lasing thresholds are computed for ring resonators with $\mathcal{F} = 1.1$ (Fig. 7(a) and 7(b)) and $\mathcal{F} = 1.5$ (Fig. 7(c) and 7(d)). In these examples we have assumed $\alpha/\gamma = 2 \times 10^{-4}$ W^2. It can be seen that for a given coupling coefficient, as αL increases both upper and lower thresholds shift to higher powers to compensate linear (for lower threshold) and nonlinear (for upper threshold) losses. We also note that although the minimum (maximum) lasing threshold at larger values of $\mathcal{F}$, becomes smaller (larger) in weakly-coupled rings.

For a given coupling coefficient the lasing power interval is larger for larger values of $\mathcal{F}$. This is shown in Fig. 8 where $\mathcal{F}$ takes four different values, 1.1, 1.25, 1.5 and 1.75. As the SBS figure of merit becomes smaller, given a constant coupling coefficient $|\kappa|$, both thresholds are increased because additional power is required to compensate the loss. In addition the threshold interval becomes smaller because the range of powers required to compensate both linear and nonlinear losses in the ring decreases. As the nonlinear loss coefficient γ approaches zero, the SBS figure of merit $\mathcal{F}$ grows without bound and the power required to attain the upper threshold
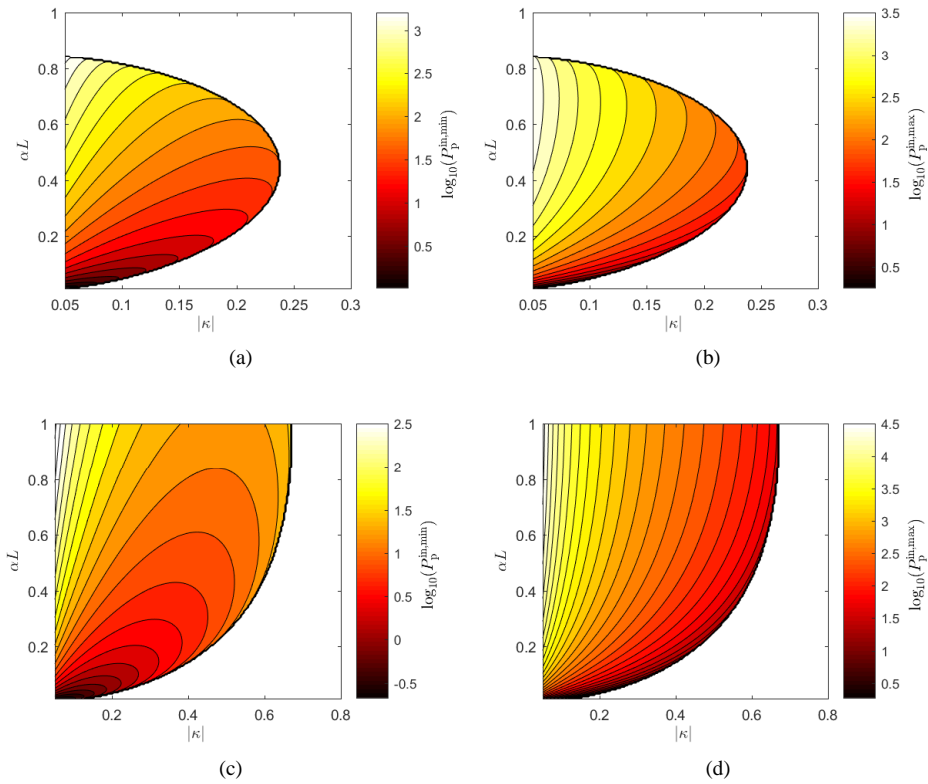
Fig. 7. Minimum/Maximum values of the lasing threshold in mW as a function of κ and αL for $\mathcal{F} = 1.1$ (a,b) and $\mathcal{F} = 1.5$ (c,d) for $\frac{\alpha}{\gamma} = 2 \times 10^{-4} \mathrm{W}^2$.

tends to infinity. While in the case of linear loss, the Stokes output steadily increases with the input pump, in rings with nonlinear loss there exists a maximum attainable Stokes power within the lasing threshold interval. The SSA can be used to estimate the corresponding pump power to the maximum Stokes in the lasing regime. The general approach is that we look for the pump power at which the round-trip gain (12) reaches its maximum within the SSA. Within this assumption, the value of G in the lasing threshold interval exceeds $1/|\tau|$, and so does not have a physical meaning (because G will be clamped by the nonlinear losses to values below $1/|\tau|$). However as a first estimate this maximum can be expected to occur at a pump power close to the true maximum value of G, because it is at this power that the overall SBS gain in the ring attains its highest value. Figure 9(a) shows the normalized pump power corresponding to the maximum output Stokes in the lasing regime as a function of αL and $\mathcal{F}$. We note that the Stokes output at this pump power is a function of the power ratio R as well as loss and SBS gain coefficients which can be in general evaluated numerically by solving Eqs. (1) and (2). The white area on left hand side of the contours is the amplification region. Figure 9(b) shows the computed value of the maximum Stokes power for a weak input Stokes power. These calculations are performed in the limit that the input Stokes is extremely weak (1 pW in these calculations), and show the maximum output power that can be obtained in the lasing regime, as a consequence of the higher-order loss terms. It can be seen that for a certain αL by increasing $\mathcal{F}$ the output Stokes first starts increasing. Whether a larger figure of merit is obtained by increasing the SBS gain or by reducing the nonlinear loss, this will lead to an increase in the round trip gain G as it shifts toward $1/|\tau|$, thereby enhancing the Stokes output. At larger values of $\mathcal{F}$ however,
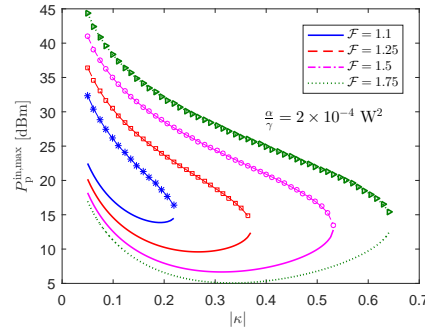
Fig. 8. Lasing thresholds as a function of the coupling coefficient for different values of $\mathcal{F}$. αL is assumed to be 0.3 and $\alpha/\gamma = 2 \times 10^{-4}$ W^2.

nonlinear losses — including small and large signal terms in Eqs.(1) and (2) — prevent further enhancement of G. Thus, the output Stokes does not change although a larger pump power is required to compensate the nonlinear losses (see Fig. 9(a)).
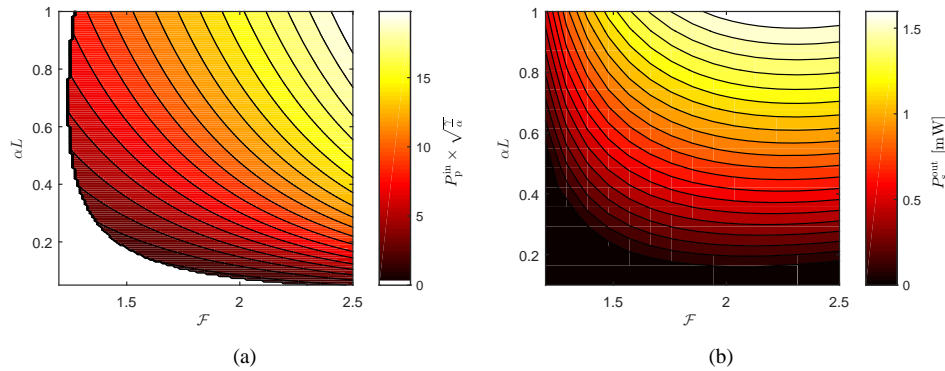

| (a) | (b) |

Fig. 9. The normalized input pump power corresponding to the maximum Stokes output in the lasing regime for a range of αL and SBS figure of merit. $|\tau|$ is assumed to be 0.9. (b) The maximum Stokes output in mW. The initial Stokes is assumed to be 1 pW.

5. Conclusion

We have investigated the physics of SBS lasing in integrated ring resonators. We provided numerical and analytic tools to evaluate the lasing threshold in rings with different SBS gains, losses and coupling properties. Moreover, useful expressions were derived and examined for the lasing threshold, and we have clarified the discussion of the distinction between lasing and amplification regimes in the case of SBS. Interestingly we found that nonlinear losses result in a finite lasing power interval, the size of which depends on the innate properties of the ring — if the properties lie outside this range then lasing will not be possible. This has consequences for experimental work that aims to design integrated structures for SBS-based lasers and applications.

Appendix: Derivation of the optical quality factor

We include here a brief derivation of the expression in Eq. (14) for the Quality factor, because it helps clarify the assumptions we have made. The pump transmission T_p of a ring resonator is given by [19]

$$T_p = \frac{(|\tau| - e^{-\frac{\alpha L}{2}})^2 + |\tau|e^{-\frac{\alpha L}{2}}(\frac{\Delta\theta}{2})^2}{(1 - |\tau|e^{-\frac{\alpha L}{2}})^2 + |\tau|e^{-\frac{\alpha L}{2}}(\frac{\Delta\theta}{2})^2}, \tag{20}$$

where $\Delta\theta = n_{eff}\Delta\omega L/C$ is the phase change over a single round trip, which is a function of frequency ω, ring length L and the effective index n_{eff} (C is the speed of light). To find the full width at half maximum (FWHM), the transmission must be equal to

$$T_p = \frac{1}{2}\left(T_{max} + T_{min}\right), \tag{21}$$

where T_{max} (T_{min}) is the maximum (minimum) pump power transmission in the spectrum, given by

$$T_{max} = \left(\frac{|\tau| + e^{-\frac{\alpha L}{2}}}{1 + |\tau|e^{-\frac{\alpha L}{2}}}\right)^2, \quad T_{min} = \left(\frac{|\tau| - e^{-\frac{\alpha L}{2}}}{1 - |\tau|e^{-\frac{\alpha L}{2}}}\right)^2. \tag{22}$$

The phase angle corresponding to the FWHM, $\Delta\theta_{FWHM}$ can then be obtained by substituting Eq. (21) in Eq. (20) and rearranging the equation

$$\Delta\theta_{FWHM} = \frac{2\sqrt{2}(1 - 1|\tau|e^{-\frac{\alpha L}{2}})}{\sqrt{1 + |\tau|^2 e^{-\alpha L}}}. \tag{23}$$

Now the Q factor can be expressed as

$$Q_L = \frac{\omega_0}{\Delta\omega_{FWHM}} = \frac{\sqrt{2}\pi L n_{eff}}{2\lambda}\frac{\sqrt{1+|\tau|^2 e^{-\alpha L}}}{1-|\tau|e^{-\frac{\alpha L}{2}}},$$

where $\Delta\omega_{FWHM}$ is the linewidth and ω_0 is the pump resonance frequency.